Article

Journal of the Brazilian Chemical Society

https://dx.doi.org/10.21577/0103-5053.20240064

J. Braz. Chem. Soc. **2024**, *35*, 9, e-20240064, 1-7

Putative Inhibitor of *Tc*CYP51 from a Library of Approved Drugs: A Virtual Screening Study

Luiz Augusto P. Flores-Junior,[a] *Eldio G. dos Santos,*[a] *Estela Maris F. Muri,*[a] *Camilo Henrique S. Lima*[b] *and Luiza Rosaria S. Dias*[*,a]

[a]*Laboratório de Química Medicinal (LQMed), Faculdade de Farmácia, Universidade Federal Fluminense, 24241-000 Niterói-RJ, Brazil*

[b]*Laboratório de Modelagem Molecular (LabMMol), Instituto de Química, Universidade Federal do Rio de Janeiro, 21941-909 Rio de Janeiro-RJ, Brazil*

Chagas disease is a public health problem, particularly in Latin America. The available treatment consists of two poorly effective drugs in the chronic phase of this parasitic disease. Considering the lack of effective treatment, alternatives are sought, such as the search focused on the biological targets of the etiologic agent. Based on this strategy, the role of *Trypanosoma cruzi* sterol 14α-demethylase (*Tc*CYP51) in ergosterol seems promising. In this work, we apply the virtual screening approach to a proposal to repurpose U.S. Food and Drug Administration (FDA)-approved drugs. We combined computational techniques and used rigorous validation to identify putative inhibitors from the FDA-approved drug library. The results indicated one of these drugs as a putative inhibitor of the *Tc*CYP51 enzyme.

Keywords: *Trypanosoma cruzi*, 14α-demethylase, virtual screening, molecular docking, ROC curve, QSAR

Introduction

Chagas disease is caused by the protozoan *Trypanosoma cruzi* (*T. cruzi*) and is transmitted by Triatominae insect vectors, infecting approximately 7 million people worldwide.[1] This disease is endemic in Latin America, where the infection occurs mainly by the bite of the vector insect or by food contaminated with the insect or its feces. Still, the transmission can also occur congenitally and by blood transfusion or organ transplantation. The treatment consists of two nitroheterocyclic drugs, benznidazole and nifurtimox, introduced around the 1970s.[1,2] Despite both being effective in the acute or early chronic infection phases, they require prolonged use, resulting in severe adverse effects and treatment withdrawal, and they are not effective at a late stage.[3,4] Therefore, there is a need to search for new antitrypanosomal agents.

In this context, drug repurposing has been highlighted in the last decade since one-third of the approved drugs were identified from this approach.[5-7] The main advantage lies in the pharmacokinetic properties and safety of preclinical models, which are well established and significantly reduce development time and investment cost.[7,8] In addition, the *in silico* drug repurposing workflow generally includes the computational approach to reduce the database size, indicating the candidates for *in vitro* or *in vivo* screening.[6-8]

Based on the research strategy on parasite-specific molecular targets, this study focused on the sterol 14α-demethylase enzyme in *Trypanosoma cruzi* (*Tc*CYP51) (EC.1.14.13.70), which acts in ergosterol biosynthesis and is essential for parasite survival.[9] We describe an *in silico* drug repurposing of U.S. Food and Drug Administration (FDA)-approved drugs using a computational approach focused on the CYP51 enzyme. We established a structure-based protocol using molecular docking to build a receiver operating characteristic curve (ROC curve) and quantitative structure-activity relationship (QSAR) to identify drugs as putative *T. cruzi* CYP51 inhibitors.

Methodology

Dataset of active compounds

Forty-eight azole compounds that exhibit activity against the amastigote forms of *T. cruzi* were taken from

*e-mail: lrsdias@id.uff.br; camilolima@iq.ufrj.br
Editor handled this article: Paula Homem-de-Mello (Associate)

the literature to build a dataset of active compounds, and their half maximal effective concentration (EC_{50}) values were converted to the negative log of half maximal effective concentration (pEC_{50}), Supplementary Information (SI) section, Tables S1-S3).[10-12] The 3D structures were built and optimized by the semi-empirical RM1 method in the Spartan 10.[13,14]

Molecular docking simulation

We obtained the crystallographic structure of the *Tc*CYP51 (PDB ID: 4C27, resolution = 1.95 Å) from PDB (Protein Data Bank).[15,16] For the molecular docking procedure, we first removed the water molecules and ions from the native structure of the protein, and the missing amino acid residues were added to the structure by the Modeller program (version 9.20).[17,18] The binding site center was defined as a sphere of 20 Å radius centered on the iron atom of the heme group (x = −10.43, y = 0.78; z = −16.30).

We used the GOLD software (Genetic Optimization for Ligand Docking, version 5.7.2) to perform the molecular docking simulations.[19] We used the ChemScore for the scoring function for the prediction of protein-ligand binding affinities.[20] We follow the given default genetic algorithm parameter values of the docking program. Each ligand was submitted to 10 docking runs, and we chose the top-ranked (highest score) docking pose from each ligand. The docking protocol was validated by re-docking, considering the root mean square deviation (RMSD) < 2 Å of the top-ranked pose.[21,22]

The analysis of intermolecular interactions and the graphic representations were generated using the Discovery Studio software (version 21.1.0.20298).[23]

Receiver operating characteristic (ROC) curve analyses

We constructed the ROC curve using the docking score of active and inactive compounds against *Tc*CYP51[24] using the Screening Explorer server.[25] In this study, we used the following statistical parameters to evaluate the performance of the ROC curve: area under the curve (AUC), total gain (TG), sensitivity (SE), and specificity (SP).[21,24,26] We also assess the probability of bias in the ROC curve by the Mann-Whitney U-test in R Commander[27] and G-Power software.[28]

This study classified 20 azole compounds with $pEC_{50} > 7.1$ as active (Table S1, SI section). Using the DecoyFinder software,[29] 200 compounds were presumed inactive from the ZINC 15 database[30,31] employing the following parameters: molecular mass (500 ± 200 Da); log P (< 6); hydrogen bonding as a donor (3 ± 1); hydrogen bonding as an acceptor (7 ± 1); rotatable bonds (7 ± 1); searching number (10 decoys for each active ligand); Tanimoto coefficient between active/decoy (0.5) and between decoy/decoy (0.5).[32,33] We built the 3D structures of the decoys using the Open Babel software[34] from a single file in the SDF format, which was separated into individual files. Hydrogen atoms were added to structures, and their energies were minimized. These structures were submitted to the docking protocol as previously described.

Construction of 3D-QSAR model

The 3D-QSAR models were developed on the active compounds dataset (Tables S1-S3, SI section) using the *per* residue energy interaction obtained from molecular docking simulations. To estimate the influence of the descriptors on the predictive capacity of the 3D-QSAR models, we built five databases (A-E), considering the following cutoff values by variance: 0.001 (A), 0.005 (B), 0.01 (C), 0.05 (D) and 0.1 (E).[35] Each database was divided into training (80%) and test (20%) sets using the supervised method of Kennard-Stone.[36] We used the combined techniques of genetic function approximation (GFA) and partial least squares (PLS) in the Wolf software[37] for the generation of QSAR equations containing 4 to 8 terms from the training sets. For this work, the following GFA parameters have been used: population size (600-1000 equations), crossover (50,000-500,000), mutation rate (100%), and smoothing factor (0.1-1.0).

Validation of 3D-QSAR equations

The equations obtained from each training set were evaluated for the correlation coefficient (R^2), the correlation leave-one-out cross-validation coefficient (Q^2), and the root-mean-square error of the estimate (RMSEE). The predicted value of R^2 (R^2_{pred}) was obtained for the test assembly as external validation.[38] The equations were selected according to the following criteria: $Q^2 > 0.5$, $R^2 > 0.6$, $R^2_{pred} > 0.5$ and RMSEE < 1.0.[38-41]

To detect possible redundancy between the descriptors, we built the cross-correlation matrix between residue and descriptors by R-Commander, discarding models with high correlation between residues (R > 0.7).[42,43]

We classified as outlier compounds from the training and the test set that presented residual value ($pEC_{50} - pEC_{50Pred}$) greater than two units of the standard deviation of the estimation (SEE).[44]

We submitted the 3D-QSAR model developed to external representativeness validation analyses for the test and training sets, model robustness, and predictive capability

through the application domain, Y-randomization, and Spearman correlation.[45,46] The application domain was calculated by ENALOS nodes in the KNIME software.[47] We used MLRPlusValidation to generate 50 models by Y-randomization calculation and analyzed the corresponding R^2 and Q^2.[48] We calculated the Spearman correlation (ρ) from the experimental and predicted values, of which weights close to 1.0 indicate a perfect correlation.[49]

Virtual screening

The 1657 FDA-approved drugs in the ZINC 15 database[31,50] were filtered and selected according to the physicochemical descriptors used for ROC curve analysis: molecular mass (500 ± 200 Da); log P (< 6); hydrogen bonding as a donor (3 ± 1); hydrogen bonding as an acceptor (7 ± 1); rotatable bonds (7 ± 1). The 3D structures of the selected compounds have been generated and minimized in the Open Babel software[34] and then submitted to the docking protocol. To identify the putative *Tc*CYP51 inhibitors, we analyzed the ROC curve based on the molecular docking score and used the 3D-QSAR model developed to predict their inhibition activity.

Results and Discussion

Despite docking helping discover new ligands, working as a filter to eliminate non-binders, and even predicting the poses of fragment-sized molecules against target site models,[51] we consider additional resources to aid in discovering new ligands. The workflow of the strategy used in virtual screening to find drugs binding the catalytic site of *Tc*CYP51 is depicted in Figure 1.

The molecular docking protocol was validated by re-docking using the co-crystallized structure of the enzyme *Tc*CYP51 complex with its inhibitor (Figure 2).[12] The RMSD of 1.58 Å obtained in re-docking agrees with the literature (< 2 Å) and is adequate for the validation of the docking protocol.[52]

We constructed a dataset containing 48 active azole compounds selected from the literature (Tables S1-S3, SI section)[10-12] and used their pEC_{50} to build the ROC curve. In the construction of the ROC curve, we used the 20 most active inhibitors (pEC_{50} > 7.1) and a set of 200 inactive compounds (decoys). The AUC-ROC (0.91) and TG (0.71) obtained (Figure 3) indicate the successful discrimination between active and inactive compounds.[24] We considered a cutoff docking score of 52.23 and analyzed the sensitivity (SE = 0.90) and specificity (SP = 0.94), demonstrating a good discriminatory capacity between active and inactive classes.

We performed an additional statistical analysis as the sampling power and normality test to identify possible bias in the ROC curve. The sampling power value obtained (1.0) indicates that the set used for ROC curve analysis was sufficient to detect relevant statistical differences since values greater than 0.8 indicate a good representation of the data used.[53,54]

We performed the normality test to estimate the ability of discrimination between the active and decoy sets,[55,56] where the active group showed a non-normal distribution (p = 0.01), and the inactive set showed a normal distribution (p = 0.08). Considering the divergent distribution, we assumed both as non-normal and performed the test based on the mean of the docking score using the non-parametric Mann-Whitney U test. This test showed a statistical difference based on the median (p-value < 0.001), indicating that the ROC curve can discriminate between active and inactive compounds. The analyses demonstrate the absence of bias in the ROC curve based on docking score and presenting representative data with discriminatory capacity.

3D-QSAR construction and validation

To predict the biological activity of potential *Tc*CYP51 inhibitors, we built a 3D-QSAR model. From the five training sets, we obtained 2700 equations that were reduced by applying the statistical cutoff criteria (Q^2, R^2, RMSEE, R^2_{pred}, and outliers) (Table 1). The variance-based descriptor

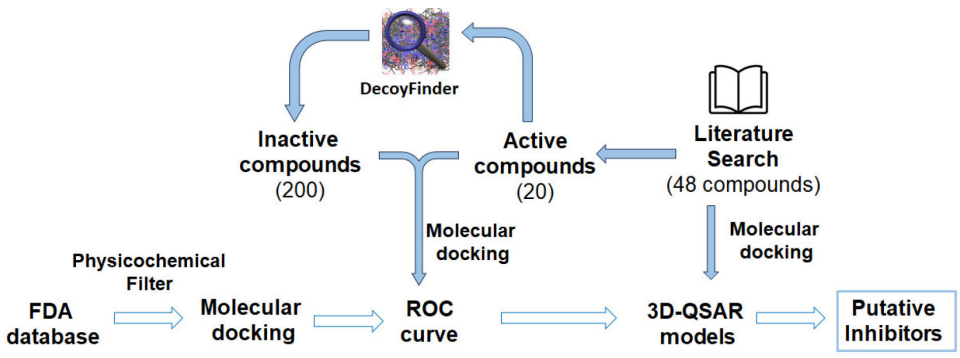

Figure 1. Workflow for virtual screening procedures adopted in this work.

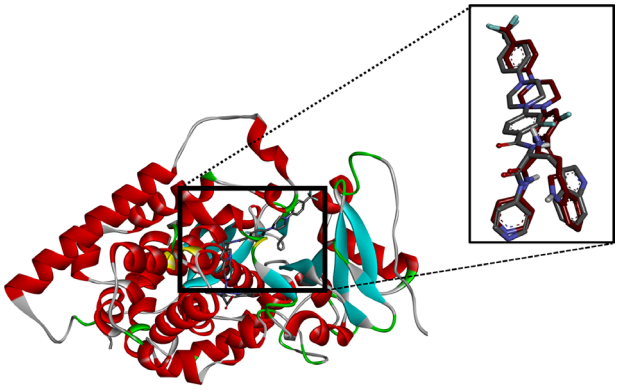

Figure 2. Superposition of 26N (grey) co-crystal structure bound to *Tc*CYP51 enzyme and the docked pose (red).

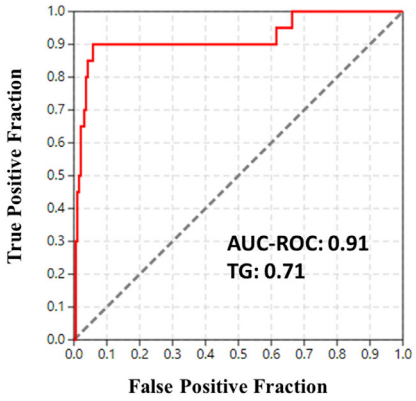

Figure 3. ROC curve and performance metrics (AUC and TG) to active and inactive compounds from docking simulation of 4C27 crystal structure.

reduction contributed to obtaining equations with adequate statistical parameters[35,39,57] since the best equation belongs to the training set with a variance cutoff of 0.05. Statistical differences between the equations may be related to the supervised method for splitting the dataset into the training and test sets, resulting in training sets with wide structural diversity.[58,59]

The training set demonstrated higher values than the cut-off criteria of this work,[38-41] with $Q^2 > 0.5$ (0.588-0.757) and $R^2 > 0.6$ (0.701-0.846) (Table 1). Considering that statistical evaluation of the test set is crucial for choosing a robust and unbiased model,[39,40,60] we used R^2_{pred} and RMSEE for the test set due to the possibility of overfitting the model. In this regard, the equations D-1, D-2, and D-3 presented acceptable values of R^2_{pred} (> 0.7) and RMSEE (≤ 0.82). Furthermore, there is no detection of outliers in equation D-3 (Table 1). Thus, as it presents the best statistical parameters to predict the biological activity of compounds not included in the training set (Table S4, SI section),[38-41,60] we selected equation D-3 ($pEC_{50} = 4.18 + 0.51 \times Met106 + 0.18 \times Tyr116 + 1.25 \times Ala211 + 0.60 \times Met358$) for the QSAR study.

The cross-correlation matrix analysis of the residual values ($pEC_{50Exp} - pEC_{50Pred}$) for independent terms of the D-3 equation showed that the residue-descriptors Met106, Tyr116, Ala211, and Met358 have low intercorrelation, indicating that the model does not present redundant information (Table 2).

We evaluated the domain application to analyze whether the prediction of the test set was reliable concerning the training set of the D-3 equation (Figure 4).[61] We used two distance-based methods, Leverage and Euclidean (domain) distances,[61,62] to analyze the training set compounds and determine a threshold value for the applicability domain (AD). Analysis of the limits generated for the training set, domain (2.48), and leverage (0.30) showed that the chemical space of the test set is comparable to the training set, without outlier compounds (Figure 4a).[61]

The evaluation of the robustness of the D-3 model was performed using Y-randomization,[63] in which the biological activity values are randomly exchanged to obtain new values of R^2 and Q^2 (Figure 4b). Analyzing the R^2 (< 0.28) and Q^2 (< 0.02) values for the 50 randomized models, we observed no random correlations between the residue descriptors and biological activity. Furthermore, the Spearman correlation coefficient for the D-3 equation

Table 1. Statistical parameters of the eight best 3D-QSAR equations generated from the training set

Training set	Equation	Terms	Q^2	R^2	R^2_{pred}	$RMSEE_{test}$	Outliers
A	1	4	0.721	0.793	0.330	0.931	2
C	1	7	0.757	0.846	0.362	0.902	3
C	2	6	0.746	0.838	0.331	0.923	3
C	3	5	0.727	0.818	0.570	0.740	2
C	4	4	0.664	0.751	0.450	0.841	3
D	1	6	0.629	0.736	0.709	0.821	2
D	2	5	0.618	0.727	0.738	0.776	2
D	3	4	0.588	0.701	0.794	0.687	0

Q^2: correlation leave-one-out cross-validation coefficient; R^2: correlation coefficient; R^2_{pred}: predicted value of correlation coefficient; $RMSEE_{test}$: root-mean-square error of the estimate of test set.

Table 2. Cross-correlation matrix of the amino acid residues from the D-3 equation

	Met106	Tyr116	Ala211	Met358
Met106	1			
Tyr116	–0.29	1		
Ala211	0.22	–0.02	1	
Met358	–0.03	–0.39	0.09	1

Ala: alanine; Met: methionine; Tyr: tyrosine.

(ρ = 0.85) indicates that the model may be suitable for biological activity estimating.[64]

Virtual screening of FDA-approved drug

To select drugs with similar characteristics to the investigated inhibitors, we used physicochemical screening parameters on the 1657 FDA-approved drugs, of which we selected 37 drugs for molecular docking and ROC curve evaluation. Our results showed that losartan[65] and imatinib[66] had significant docking scores (52.53), above the cutoff value (52.23) (Table S5, SI section). Also, we tested the AD analysis to indicate whether the D-3 equation descriptors were reliable for predicting biological activity for both drugs. However, the AD value of losartan (1.57) and imatinib (2.83) suggest that the losartan prediction was reliable while imatinib was not, indicating that only losartan retains chemical characteristics like the training and test set.[33,67,68] Then, we used the D-3 equation to obtain the predicted activity value for losartan (pEC_{50} = 8.04).

Our results showed similar interactions between the *Tc*CYP51 binding site residues and the most active inhibitor in the database (27) (Tables S1-S3, SI section) or losartan, observed by the normalized energy values of equation D-3. They suggested the interaction of losartan with the cofactor due to the proximity of the tetrazole ring to Fe-Heme (d = 2.5 Å). Comparison with amino acid residues from the D-3 equation suggests that interactions with Met106 and Met358 are meaningful for the predicted activity since losartan and compound 27 follow the same trend (Figure 5). Interestingly, losartan has already been reported as relevant in Chagas disease by treating heart failure in patients with Chagas cardiomyopathy.[69,70]

Conclusions

In this work, we developed a ROC curve and a QSAR model to identify putative TcCYP51 inhibitors by virtual screening. Based on the docking score value (52.53) by the ChemScore function of the GOLD software, the

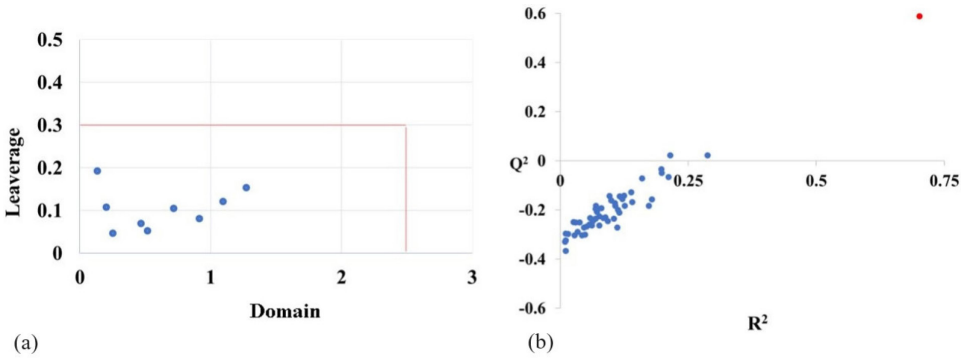

Figure 4. (a) Applicability domain plot for the test set of equation D-3. (b) Y-randomization plot for D-3 equation: original model (red ball) and the 50 randomized models (blue balls).

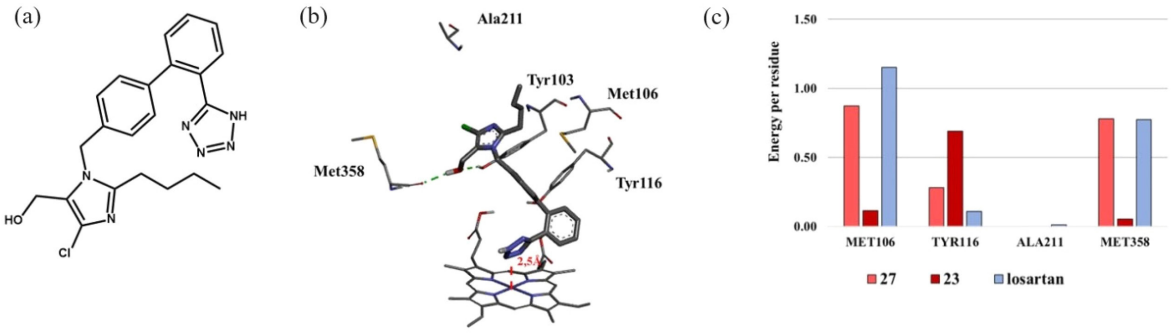

Figure 5. (a) 2D chemical structure of losartan. (b) 3D intermolecular interactions obtained by molecular docking between losartan and *Tc*CYP51 binding site residues. Hydrogen bond (green dashed line); the distance between the Fe-Heme and *N*-tetrazole ring (red dashed line). (c) The graph of energies *per* residue of losartan and compounds 23 and 27 from the QSAR study. Ala: alanine; Met: methionine; Tyr: tyrosine.

ROC curve showed an excellent discrimination capacity (AUC: 0.919; TG: 0.71; SE: 0.9 and SP: 0.94). The energy *per* residue used as a descriptor to build the 3D-QSAR model presented suitable statistical parameters (Q2: 0.588; R2: 0.701; RMSEE: 0.633) without outliers for training and test sets.

Our virtual screening of the FDA-approved drugs database, following the traced physicochemical properties, the ROC-curve, and the developed 3D-QSAR model, indicated losartan drug as a putative inhibitor of *Tc*CYP51, showing a reliable prediction estimate in the model QSAR. The results suggest this drug is a candidate for further studies as a trypanocide agent or a lead compound in designing new *Tc*CYP51 inhibitors.

Supplementary Information

Supplementary information (Tables S1-S5) is available free of charge at http://jbcs.sbq.org.br as PDF file.

Acknowledgments

The authors are grateful for the financial support of the following Brazilian funding agencies: CAPES, finance code 001, and their granting of a graduate scholarship to the first author; and FAPERJ (E-26/210.915/2021), and their granting of a graduate scholarship to the second author (E-26/204.137/2022).

Author Contributions

Luiz Augusto P. Flores-Júnior was responsible for investigation, methodology, writing original draft; Eldio G. dos Santos for investigation; Estela Maris F. Muri for investigation; Camilo H. S. Lima for conceptualization, project administration, supervision, writing original draft; Luiza Rosaria S. Dias for conceptualization, project administration, supervision, writing review and editing.

References

1. World Health Organization (WHO); *Chagas Disease (also known as American trypanosomiasis)*, https://www.who.int/news-room/fact-sheets/detail/chagas-disease-(american-trypanosomiasis), accessed in April 2024.
2. Pérez-Molina, J. A.; Crespillo-Andújar, C.; Bosch-Nicolau, P.; Molina, I.; *Enfermedades Infecciosas Microbiologia Clinica* **2021**, *39*, 458. [Crossref]
3. Oliveira, G. B. F.; Avezum, A.; Cordeiro, M. A. J.; *Global Heart* **2015**, *10*, 189. [Crossref]
4. Bermudez, J.; Davies, C.; Simonazzi, A.; Real, J. P.; Palma, S.; *Acta Trop.* **2016**, *156*, 1. [Crossref]
5. Talevi, A.; Bellera, C. L.; *Expert Opin. Drug Discovery* **2020**, *15*, 397. [Crossref]
6. Hernandez, H. W.; Soeung, M.; Zorn, K. M.; Ashoura, N.; Mottin, M.; Andrade, C. H.; Caffrey, C. R.; Siqueira-Neto, J. L.; Ekins, S.; *Pharm. Res.* **2019**, *36*, 27. [Crossref]
7. GNS, H. S.; GR, S.; Murahari, M.; Krishnamurthy, M.; *Biomed. Pharmacother*. **2019**, *110*, 700. [Crossref]
8. Pushpakom, S.; Iorio, F.; Eyers, P. A.; Escott, K. J.; Hopper, S.; Wells, A.; Doig, A.; Guilliams, T.; Latimer, J.; McNamee, C.; Norris, A.; Sanseau, P.; Cavalla, D.; Pirmohamed, M.; *Nat. Rev. Drug Discovery* **2019**, *18*, 41. [Crossref]
9. Sueth-Santiago, V.; Franklim, T. N.; Lopes, N. D.; Lima, M. E. F.; *Rev. Virtual Quim*. **2015** *7*, 539. [Crossref]
10. Andriani, G.; Amata, E.; Beatty, J.; Clemets, Z.; Coffey, B. J.; Courtemanche, G.; Devine, W.; Erath, J.; Juda, C. E.; Wawrzak, Z.; Wood, J. T.; Lepesheva, G. I.; Rodriguez, A.; Pollastri, M. P.; *J. Med. Chem*. **2013**, *56*, 2556. [Crossref]
11. Calvet, C. M.; Vieira, D. F.; Choi, J. Y.; Kellar, D.; Cameron, M. D.; Siqueira-Neto, J. L.; Gut, J.; Johnston, J. B.; Lin, L.; Khan, S.; McKerrow, J. H.; Roush, W. R.; Podust, L. M.; *J. Med. Chem.* **2014**, *57*, 6989. [Crossref]
12. Vieira, D. F.; Choi, J. Y.; Calvet, C. M.; Siqueira-Neto, J. L.; Johnston, J. B.; Kellar, D.; Gut, J.; Cameron, M. D.; McKerrow, J. H.; Roush, W. R.; Podust, L. M.; *J. Med. Chem.* **2014**, *57*, 10162. [Crossref]
13. Dewar, M. J. S.; Zoebisch, E. G.; Healy, E. F.; Stewart, J. J. P.; *J. Am. Chem. Soc.* **1985**, *107*, 3902. [Crossref]
14. *Spartan'10*, version 10; Wavefunction, USA, 2010.
15. Goodsell, D. S.; Zardecki, C.; Di Costanzo, L.; Duarte, J. M.; Hudson, B. P.; Persikova, I.; Segura, J.; Shao, C.; Voigt, M.; Westbrook, J. D.; Young, J. Y.; Burley, S. K.; *Protein Sci*. **2020**, *29*, 52. [Crossref]
16. Protein Data Bank, https://www.rcsb.org/structure/4C27, accessed in April 2024.
17. Webb, B.; Sali A.; *Modeller*, version 10.4; University of California, USA, 2018.
18 Eswar, N.; Webb, B.; Marti-Renom, M. A.; Madhusudhan, M. S.; Eramian, D.; Shen, M.; Pieper, U.; Sali, A.; *Curr. Protoc. Protein Sci.* **2007**, *2*, 2. [Crossref]
19. *GOLD*; Cambridge Crystallographic Data Centre, UK, 2023.
20. Verdonk, M. L.; Cole, J. C.; Hartshorn, M. J.; Murray, C. W.; Taylor, R. D.; *Proteins: Struct., Funct., Bioinf.* **2003**, *52*, 609. [Crossref]
21. Triballeau, N.; Acher, F.; Brabet, I.; Pin, J.-P.; Bertrand, H.-O.; *J. Med. Chem*. **2005**, *48*, 2534. [Crossref]
22. Lima, C. H. S.; Soares, J. C. A. V.; Ribeiro, J. L. S.; Muri, E. M. F.; de Albuquerque, S.; Dias, L. R. S.; *Lett. Drug Des. Discovery* **2020**, *17*, 184. [Crossref]
23. *BIOVIA Discovery Studio Visualizer*, version 21.1.0.20298; Datassault Systèmes, USA, 2020.
24. Empereur-Mot, C.; Zagury, J. F.; Montes, M.; *J. Chem. Inf. Model*. **2016**, *56*, 2281. [Crossref]

25. Screening Explorer, *Screening Results Analysis Online*, http://stats.drugdesign.fr/, accessed in Aprilr 2024.
26. Schuler, J.; Falls, Z.; Mangione, W.; Hudson, M. L.; Bruggermann, L.; Samudrala, R.; *Drug Discovery Today* **2022**, *27*, 49. [Crossref]
27. Fox, J.; Marquez, M. M.; Boucget-Valat, M.; *Rcmdr: R Commander*; USA, 2024.
28. Faul, F.; Erdfelder, E.; Lang, A.-G.; Buchner, A.; *G*Power 3*, version 3.1.3; Universität Kiel, Switzerland, 2010.
29. Adrià, C. M.; Garcia-Vallvé, S.; Pujadas, G.; *DecoyFinder* v. 2.0, Spain, 2007.
30. ZINC15, https://zinc15.docking.org/substances/table.html, accessed in April 2024.
31. Sterling, T.; Irwin, J. J.; *J. Chem. Inf. Model*. **2015**, *55*, 2324. [Crossref]
32. Cereto-Massagué, A.; Guasch, L.; Valls, C.; Mulero, M.; Pujadas, G.; Garcia-Vallvé, S.; *Bioinformatics* **2012**, *28*, 1661. [Crossref]
33. Azevedo, P. H. R. A.; Peçanha, B. R. B.; Flores-Junior, L. A. P.; Alves, T. F.; Dias, L. R. S.; Muri, E. M. F.; Lima, C. H. S.; *J. Biomol. Struct. Dyn*. **2023**, *42*, 1417. [Crossref]
34. *Open Babel* 3-1-1; The Open Babel Team, Boston, USA,, 2020. [Link] accessed in April 2024
35. Araújo, J. Q.; de Brito, M. A.; Hoelz, L. V. B.; Alencastro, R. B.; Castro, H. C.; Rodrigues, C. R.; Alburquerque, M. G.; *Eur. J. Med. Chem.* **2011**, *46*, 39. [Crossref]
36. Snarey, M.; Terrett, N. K.; Willett, P.; Wilton, D. J.; *J. Mol. Graphics Modell*. **1997**, *15*, 372. [Crossref]
37. Rogers, D.; *WOLF*, version 6.2; The Chem21 Group Inc., USA, 1994.
38. Gramatica, P. In *Computational Toxicology*, vol. II; Reisfeld, B.; Mayeno, A. N. eds.; Humana Press - Springer: New York, USA, 2013, ch. 21. [Crossref]
39. De, P.; Kar, S.; Ambure, P.; Roy, K.; *Arch. Toxicol.* **2022**, *96*, 1279. [Crossref]
40. Peter, S. C.; Dhanjal, J. K.; Malik, V.; Radhakrishnan, N.; Jayakanthan, M..; Sundar, D.; In *Encyclopedia of Bioinformatics and Computational Biology*; Ranganathan, S.; Gribskov, M.; Nakai, K.; Schönbach, C., eds.; Academic Press: Oxford, 2019, p. 661. [Crossref]
41. Tropsha, A.; *Mol. Inf.* **2010**, *29*, 476. [Crossref]
42. Fox, J.; *J. Stat. Software* **2005**, *14*, 1. [Crossref]
43. Rácz, A.; Bajusz, D.; Héberger, K.; *Molecules* **2019**, *24*, 2811. [Crossref]
44. Rogers, D.; Hopfinger, A. J.; *J. Chem. Inf. Model*. **1994**, *34*, 854. [Crossref]
45. Vrontaki, E.; Melagraki, G.; Mavromoustakos, T.; Afantitis, A.; *J. Enzyme Inhib. Med. Chem*. **2016**, *31*, 38. [Crossref]
46. Rajput, A.; Kumar, A.; Kumar, M.; *Front. Pharmacol*. **2019**, *10*, 71. [Crossref]
47. *Enalos Nodes for KNIME*; NovaMechanics Ltd., Cyprus, 2023.
48. Roy, K.; Mitra, I.; *Comb. Chem. High Throughput Screening* **2011**, *14*, 450. [Crossref]
49. Szmidt, E.; Kacprzyk, J. In *Computational Intelligence for Knowledge-Based Systems Design,* vol. 6178; Hüllermeier, E.; Kruse, R.; Hoffmann, F., eds.; Springer: Berlin, Heidelberg, 2010. [Crossref]
50. ZINC15, https://zinc15.docking.org/catalogs/dbfda/, accessed in April 2024.
51. Kolb, P.; Irwin, J. J.; *Curr. Top. Med. Chem.* **2009**, *9*, 755. [Crossref]
52. Hevener, K. E.; Zhao, W.; Ball, D. M.; Babaoglu, K.; Qi, J.; White, S. W.; Lee, R. E.; *J. Chem. Inf. Model*. **2009**, *49*, 444. [Crossref]
53. Mishra, P.; Pandey, C.; Singh, U.; Gupta, A.; Sahu, C.; Keshri, A.; *Ann. Card. Anaesth.* **2019**, *22*, 67. [Crossref]
54. Patino, C. M.; Ferreira, J. C.; *J. Bras. Pneumol*. **2016**, *42*, 162. [Crossref]
55. Kennedy-Shaffer, L.; *Am. Stat*. **2019**, *73*, 82. [Crossref]
56. Greenland, S.; Senn, S. J.; Rothman, K. J.; Carlin, J. B.; Poole, C.; Goodman, S. N.; Altman, D. G.; *Eur. J. Epidemiol*. **2016**, *31*, 337. [Crossref]
57. Yoo, C.; Shahlaei, M.; *Chem. Biol. Drug Des.* **2018**, *91*, 137. [Crossref]
58. Andrada, M. F.; Vega-Hissi, E. G.; Estrada, M. R.; Martinez, J. C. G.; *SAR QSAR Environ. Res*. **2017**, *28*, 1011. [Crossref]
59. Xu, Y.; Goodacre, R.; *J. Anal. Test.* **2018**, *2*, 249. [Crossref]
60. Kolmar, S. S.; Grulke, C. M.; *J. Cheminf.* **2021**, *13*, 92. [Crossref]
61. Roy, K.; Kar, S.; Ambure, P.; *Chemom. Intell. Lab. Syst*. **2015**, *145*, 22. [Crossref]
62. Sahigara, F.; Mansouri, K.; Ballabio, D.; Mauri, A.; Consonni, V.; Todeschini, R.; *Molecules* **2012**, *17*, 4791. [Crossref]
63. Rücker, C.; Rücker, G.; Meringer, M.; *J. Chem. Inf. Model*. **2007**, *47*, 2345. [Crossref]
64. Fourches, D.; Muratov, E.; Ding, F.; Dokholyan, N. V.; Tropsha, A.; *J. Chem. Inf. Model*. **2013**, *53*, 1915. [Crossref]
65. Sica, D. A.; Gehr, T. W. B.; Ghosh, S.; *Clin. Pharmacokinet.* **2005**, *44*, 797. [Crossref]
66. Peng, B.; Lloyd, P.; Schran, H.; *Clin. Pharmacokinet.* **2005**, *44*, 879. [Crossref]
67. Gramatica, P.; *QSAR Comb. Sci*. **2007**, *26*, 694. [Crossref]
68. Weaver, S.; Gleeson, M. P.; *J. Mol. Graph Model*. **2008**, *26*, 1315. [Crossref]
69. Souza-Silva, T. G.; Diniz, L. F.; Mazzeti, A. L.; Mendonça, A. A. S.; Gonçalves, R. V.; Novaes, R. D.; *Parasitology* **2019**, *146*, 914. [Crossref]
70. Torres, R. M.; Correia, D.; Nunes, M. C. P.; Dutra, W. O.; Talvani, A.; Sousa, A. S.; Mendes, F. S. N. S.; Scanavacca, M. I.; Pisani, C.; Moreira, M. C. V.; Junior, W. O.; Martins, S. M.; Dias, J. C. P.; *Mem. Inst. Oswaldo Cruz.* **2022**, *117*, e210172. [Crossref]

Submitted: October 17, 2023
Published online: April 23, 2024